2023 8th International Conference on
Advanced Robotics and Mechatronics
July 8-10, Sanya, China

Design, Optimization and Analysis of a Novel Compliant Guiding Mechanism for Piezo-Driven Vibration Microinjection

Yitong Li[1], Tingting Ye[2], Jie Ling[3], Xiaohui Xiao[1] and Zhao Feng[1]

2023 International Conference on Advanced Robotics and Mechatronics (ICARM) | 979-8-3503-0017-8/23/$31.00 ©2023 IEEE | DOI: 10.1109/ICARM58088.2023.10218809

Abstract— **Cell microinjection, as a significant tool of biomedical research, calls for advanced equipment with high efficiency, high success rate, high reliability, and repeatability. With the intent of providing a useful manipulator for robotic cell microinjection, this paper presents a novel complaint guiding mechanism for piezo-driven vibration cell microinjection. Mechanism design, kinematic modeling, parametric optimization, and simulation of the designed guiding mechanism are introduced in detail. The compliant guiding mechanism has a symmetrical and parallel connection structure with lumped compliance at its double-notch right-circle flexure hinges. Aiming at avoiding the resonance of the mechanism at actuation frequency, the response surface algorithm is utilized to optimize the dominant structural parameters of the designed guiding mechanism based on kinematic modeling with the pseudo-rigid-body method. The finite element simulation results show that the optimized compliant mechanism has the advantages of high off-axis stiffness and ideal working performance at the actuation frequency of 15 kHz, where the output amplitude of in-plane and out-of-plane lateral vibrations are diminished to 40% and 25% of the input lateral vibration amplitude respectively.**

I. INTRODUCTION

A cell is the elementary structure and functional unit composing living organisms. With the propelling of the research demand of biology science, micromanipulation technology for cells has been experiencing rapid development in the past few decades [1]. Cell microinjection is a convenient approach to realize the infusion of quantitative foreign materials (e.g., drug compounds, protein, DNA, RNAi, sperms) into the object living cells [2]. Compared with other methods of cell materials transmission such as carrier transport and chemical agents delivery, the microinjection technique has the distinct advantages of low toxicity, high efficiency, and the ease of rationing the volume of materials. Therefore, cell microinjection has been widely used in biomedical areas such as genetics [3], transgenics [4], and intracytoplasmic sperm injection (ICSI) [5].

As the most extensive practice in biological research, conventional manual cell microinjection conducts cell penetration and infusion process under microscopes by trained operators [6]. However, the skill and experience of the operator play a key role in accomplishing a successful injection process that is attentively demanding, fatigue-causing, time-consuming, and difficult to be replicated [7]. Due to the strict conditions including a suitable target point, appropriate trajectory of the fine needle, effectual injection speed, and well-thought-out force variation [8], it takes a very long time to train a skilled operator [9]. Furthermore, even for an experienced operator, the success rate of the injection and the survival rate of the cells can only reach around 15% [10]. Therefore, there is an urgent need to develop robotic cell microinjection systems [11]–[14] for releasing human labor, conducting batch injection, increasing the success rate, and reducing cell deformation to guarantee survival rate.

According to the different penetrating strategies, robotic microinjectors are generally divided into three categories, i.e., direct penetration, rotation drilling penetration, and vibration penetration. Microinjectors with direct penetration strategies have a relatively large motion range, but large deformation of the cell could be easily caused at the same time. For example, Wang et al. [15] designed a piezo-driven microinjector with a bridge-type displacement amplifier, which can generate a maximum displacement of up to 301 μm and the survival rate exceeded 80% according to the report. Rotationally penetrating microinjectors are usually actuated by DC motors. For instance, Ergenc et al. [16] proposed a rotationally oscillating drill integrating a DC motor and flexure precision bearings and obtained a success rate over 70%. However, some eccentricity and whirling motion that is harmful to the cells are inevitable during the rotational oscillation.

Mainly composed of phospholipid elastic semi-permeable membrane, cell membrane fulfils a vital function of separating and protecting a cell from its surrounding environment [17]. The cell membrane shows a defining characteristic of viscoelasticity, leading to great difficulties in puncturing the membrane while restraining its deformation to ensure the survival of the cell. To tackle this problem, vibration penetration method was promoted because of its capability to penetrate the cell membrane with a much smaller displacement of the micropipette. Under the longitudinal vibration with high frequency and small amplitude of the micropipette, when the strain energy of the viscoelastic membrane achieves its yield limit, the cell membrane can be punctured successfully and deformed slightly in the meanwhile. The crucial challenge of vibration penetration is to conduct an appropriate axial vibration and suppress the consequent lateral vibration. The seminal work of Ediz et al. [18] provides a landmark of

*This work was supported by National Natural Science Foundation of China (Grant No. 51375349) and Natural Science Foundation of Jiangsu Province (Grant No. BK20210294)

[1]Yitong Li, Xiaohui Xiao and Zhao Feng are with the School of Power and Mechanical Engineering, Wuhan University, Wuhan, 430072, China {lyt37729, xhxiao, fengzhao}@whu.edu.cn

[2]Tingting Ye is with the Department of Industrial and Systems Engineering, The Hong Kong Polytechnic University, Hong Kong SAR 999077, China tilda.ye@connect.polyu.hk

[3]Jie Ling is with the College of Mechanical and Electrical Engineering, Nanjing University of Aeronautics and Astronautics, Nanjing 210016, China meejling@nuaa.edu.cn

vibration cell injection. The injector tip's lateral vibration amplitude was decreased to $\pm 135 \mu m$ in the air by introducing mercury into the micropipette, but mercury is toxic for cells to some extent. On this basis, several injectors for vibration penetration are developed successively for smaller lateral vibration amplitudes and lower toxicity. For example, Huang et al. [19] presented a piezo-driven ultrasonic cell injection system without the use of a mercury column and cut down the harmful lateral vibration amplitude to $\pm 39 \mu m$ in the air by centralizing the oscillation power near the injector pipette; Johnson et al. [20] proposed a flexure-guided piezo drill which adopted a compliant mechanism with parallelogram arrangement to decline the lateral vibration amplitude effectively. To sum up, a variety of microinjectors for biomedical fields have been proposed and investigated for structure optimization and control strategies. But so far, they are mostly at the developing stage and the performance still needs promotion until they can be put into practice broadly. Previous studies have revealed the superiority of vibration penetration strategy, but few work paid attention to the suppression of the harmful excessive lateral vibration. Therefore, it is necessary to devise a new microinjector that can facilitate the cell injection process and raise the success rate.

Motivated by flexure-guided vibration microinjectors, this paper presents a novel vibration microinjector composed of a piezoelectric actuator (PEA) and a compliant guiding mechanism for restraining lateral vibration. Piezo-driven compliant mechanisms have the merits of small size, lightweight, few steps of assembly, no friction, and ease of control [21], [22]. The designed guiding mechanism shows an innovative structure which is utilized to guide straight-line movements. It is proven that this novel guiding mechanism can suppress lateral vibration in a both valid and non-toxic way. The main contributions of this paper lie in:

- A novel compliant guiding mechanism as well as its kinematic modeling is devised and developed to guide the axial movement and restrain lateral vibration.
- Dominant parameters are optimized through the response surface algorithm.
- Finite element analysis is introduced with the intent of assessing the performance of the optimized guiding mechanism. It shows that the undesired lateral vibration can be effectively weakened by the proposed compliant guiding mechanism.

The structure of this paper is arranged as follows. The mechanism design will be introduced in section II. The kinematic modeling and parametric optimization will be presented in section III. The performance of the optimized guiding mechanism will be assessed in section IV. Finally, the conclusions will be offered in section V.

II. MECHANISM DESIGN

Because of the asymmetry caused by limited manufacturing precision, inevitable misalignment in assembly, and other disturbances, lateral vibration will be transmitted to the micropipette's tip in piezo-driven microinjectors. To diminish the cell deformation and damage in the process of robotic cellular membrane penetration, the compliant guiding mechanism is expected to guide the glass micropipette along the actuation direction, which means suppressing the output lateral vibration and achieving an appropriate axial vibration amplitude in the meanwhile.

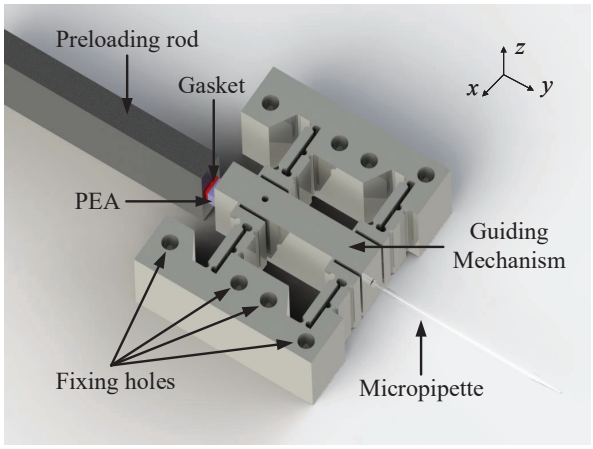

Fig. 1. Computer-aided design model of the proposed compliant piezo-driven microinjector.

Research on cell vibration injection has shown that a higher success rate and cellular survival rate can be achieved under appropriate driven frequency, suitable axial vibration amplitude, and restricted lateral vibration amplitude of the injection device. To penetrate the membrane of an oocyte or embryo, it is feasible to adopt the vibration penetrating strategy when the driven frequency is from 15 to 18 kHz in the light of previous reports [20], [23]. It has been deemed that the required axial vibration amplitude depends on the size of the target cell, and the lateral vibration amplitude in the air is preferably limited under 2 μm.

The computer-aided model (CAD) of the designed compliant piezo-driven microinjector is shown in Fig. 1. The microinjector is comprised of a guiding mechanism based on lumped compliance, a sharp micropipette made of borosilicate glass, a PEA, a gasket, and an adjustable pre-tightening rod. Piezoelectric actuators are widely used in compliant manipulators because of their advantages of high resolution, fast response, high stiffness, and ease of integration in miniaturized devices. The PEA is employed symmetrically behind the guiding mechanism and its output force and displacement are along the axis of the guiding mechanism and the micropipette so that the axial vibration can be transmitted adequately to the micropipette's tip. The gasket and the preloading rod are employed to meet the requirements of applying the PEA properly.

The guiding mechanism is designed as a symmetrical and parallel connection structure with lumped compliance at its compliant joints. Double-notch right-circular flexure hinge with a single axis is adopted owing to its high out-of-plane stiffness. One of the evident discrepancies between circular flexure hinges and other types of flexure hinges is that the circular hinge has a comparatively low motion range [24].

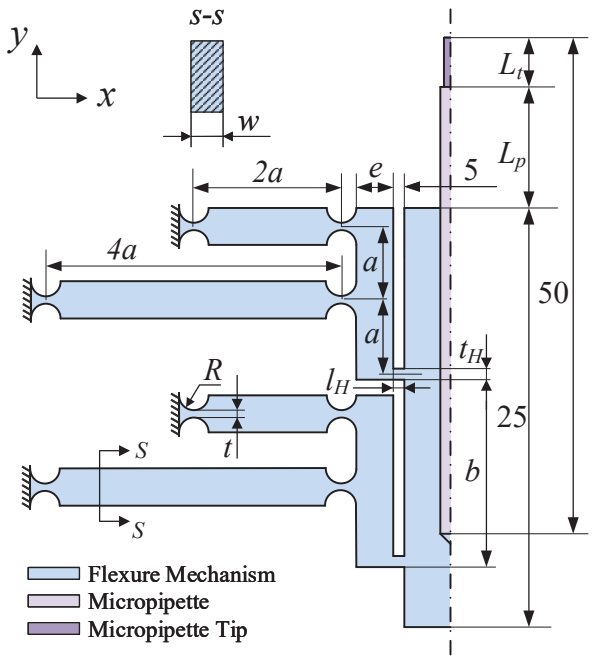

Fig. 2. Structural parameters of the compliant guiding mechanism.

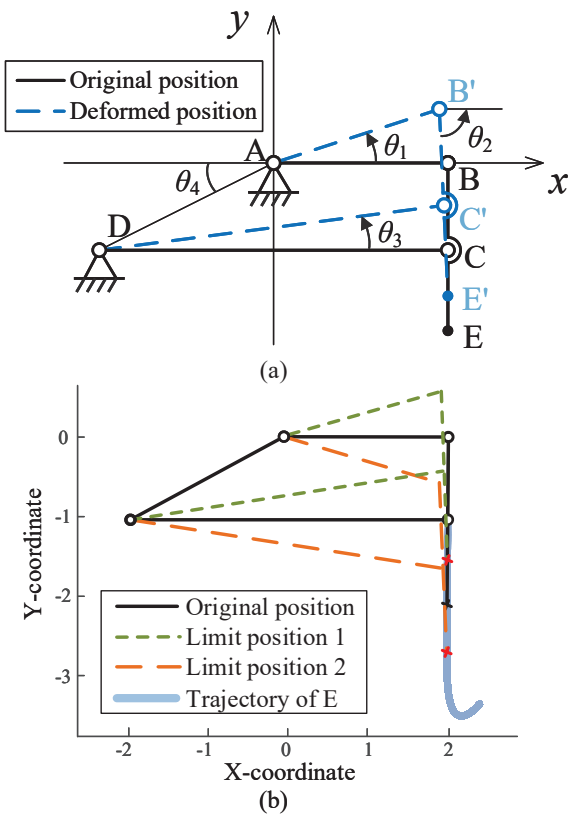

Fig. 3. The pseudo-rigid body model of the straight-line module: (a) the analytical kinematic model, (b) the positions of the pseudo-rigid bars and the trajectory of its endpoint calculated by MATLAB.

In the case of this mechanism, the working stroke is on a micron scale and the flexure hinges rotate in a small angle range. Hence the circular profile suits the requirements of this design well. There are four identical compliant modules that can generate approximate straight-line motion at their endpoints. Because the rotation movements of these endpoints will be generated simultaneously, the parallel connection structure is adopted to conduct a straight-line motion to the micropipette. Moreover, the parallel structure has many merits such as high accuracy, high stiffness, small size, and symmetry. In addition, the symmetrical placement is adopted in order to eliminate the parasitic movement theoretically and to increase the lateral stiffness of the compliant guiding mechanism.

The guiding mechanism can be manufactured by wire electrical discharge machining (EDM) owing to the monolithic structure. Spring steel was chosen to construct the guiding mechanism because of its high yield strength (784 MPa).

III. KINEMATIC MODELING AND PARAMETRIC OPTIMIZATION

A. Kinematic Modeling of Straight-line Module

The contour of the compliant guiding mechanism and the meaning of its main design parameters are shown in Fig. 2. The design variables are selected as $a, b, e, R, t, w, t_H, l_H$. The constraint conditions are brought by the geometry space limitations of each element, which can be described as

$$a > t + 2R, \tag{1}$$

$$2a + \frac{t_H + t}{2} + R + b < 25. \tag{2}$$

The circular flexure hinges are utilized to connect the contiguous rigid elements. Each flexure hinge constitutes a revolute joint attached with a torsional spring, the pseudo-rigid body model (PRBM) of the straight-line guiding module is demonstrated in Fig. 3(a), regardless of the rotation centers' draft. A, B, C, D, E are the rotation center. $\theta_i (i = 1, 2, 3, 4)$ is the angle between the pseudo-rigid link and the x axis in rigid-body coordinate system. The end point E is expected to move in a straight line that is parallel to the y axis. According to the geometric conditions, the following equations can be obtained:

$$\tan\theta_4 = \frac{1}{2}, \tag{3}$$

$$2a \cdot \sin\theta_1 - a \cdot \sin\theta_2 = -\sqrt{5}a \cdot \sin\theta_4 + 4a \cdot \sin\theta_3, \tag{4}$$

$$2a \cdot \cos\theta_1 + a \cdot \cos\theta_2 = -\sqrt{5}a \cdot \cos\theta_4 + 4a \cdot \cos\theta_3. \tag{5}$$

Combining (3), (4) and (5), θ_2 and θ_3 can be expressed as a function of θ_1. Therefore, the coordinate of the end point E are,

$$x_E = 2a \cdot \cos\theta_1 + 2a \cdot \cos\theta_2 = \varphi(\theta_1), \tag{6}$$

$$y_E = 2a \cdot \sin\theta_1 - 2a \cdot \sin\theta_2 = \psi(\theta_1). \tag{7}$$

Then, the curvature k of the trajectory of E can be calculated as:

$$k = \frac{\varphi'(\theta_1)\psi''(\theta_1) - \psi'(\theta_1)\varphi''(\theta_1)}{\left[\varphi'^2(\theta_1) + \psi'^2(\theta_1)\right]^{3/2}}. \tag{8}$$

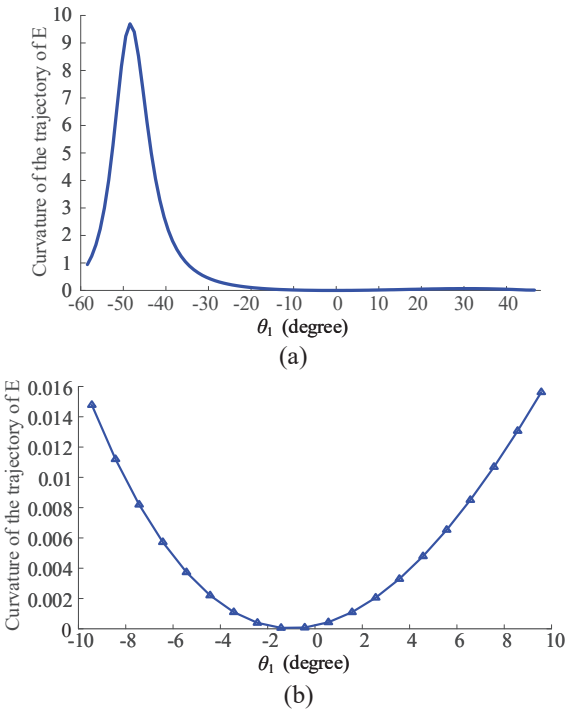

Fig. 4. The curvature of the trajectory of the end point E:(a) θ_1 ranges from $-58^\circ \sim 46^\circ$, (b) θ_1 ranges from $-10^\circ \sim 10^\circ$.

The kinematic analytical modeling was calculated through the software MATLAB. Let a equal 1, the depicted trajectory is shown in Fig. 3(b). The value of its curvature k is demonstrated in Fig. 4. The analytical results indicate that the curvature is less than 0.016 when θ_1 ranges from -10° to 10°, which proves that the endpoint E is moving in a straight line approximately.

B. Optimization of Design Parameters

With the purpose of avoiding the resonance of the designed microinjector, the natural frequency of the guiding mechanism should not be too close to the actuation frequency ranging from 15 to 18 kHz. Design parametric optimization based on response surface algorithms through simulation calculation is adopted to acquire a feasible guiding mechanism with appropriate frequency characteristics. The structural parameter array $[R, b, w, e, a]$ is selected to be the input design variable, the physical meaning is denoted in Fig. 2. The optimization design constraints are (1) and (2). The thickness of the double-notch right circular hinges t is set as 0.4 mm given the mechanism's service lifetime and the limited manufacturing capacity. The optimization goal is selected as the maximization of the second-order natural frequency of the compliant guiding mechanism. The input value range of each parameter and the optimization results are shown in Table I.

The design variables' sensitivity to the guiding mechanism's first-two natural frequencies is obtained by the response surface analysis, which indicates the extent of influence of each structure parameter on the objective function. Design variable with a higher absolute value of sensitivity has a larger impact on the natural frequencies. The sensitivity values are listed in Table I and its column diagram is shown in Fig. 5. It can be seen that e and a are the primary factors affecting the second-order natural frequency of the guiding mechanism, and the first-order natural frequency decreases with the increase of R, W, e, a. The dynamic performance of the optimized compliant guiding mechanism is significantly better than before.

TABLE I
THE PARAMETRIC OPTIMIZATION OF THE GUIDING MECHANISM

Parameter	Value Range (mm)	Optimized Value (mm)	1st orders' Sensitivity	2nd orders' Sensitivity
R	[0.4, 0.6]	0.5	-0.634	0
b	[10, 16]	16	0	0
w	[12, 16]	14	-0.579	0
e	[1.2, 1.7]	1.6	-0.349	0.266
a	[2, 2.5]	2	-0.486	-0.269

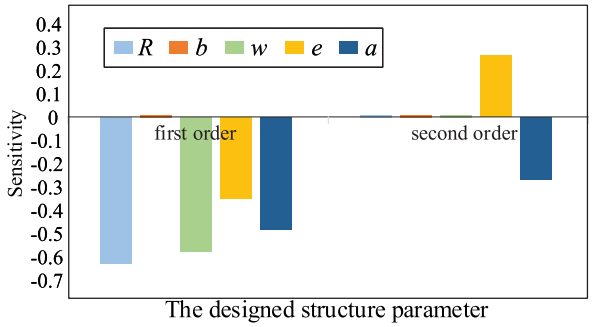

Fig. 5. The contribution of each design variable on the first-two natural frequencies of the compliant guiding mechanism.

TABLE II
COMPUTATION OF FINITE ELEMENT STRUCTURAL SIMULATION

k_x $(N/\mu m)$	k_y $(N/\mu m)$	k_z $(N/\mu m)$	k_x/k_y	k_z/k_y
248.88	21.91	324.15	11.36	14.79

IV. FEA SIMULATION STUDY OF THE GUIDING MECHANISM

A. Static and Modal Simulation

To verify the performance of the optimized guiding mechanism, the finite element analysis (FEA) is conducted through the software ANSYS Workbench. The structure parameters R, b, w, e, a are chosen as 0.5mm, 16mm, 14mm, 1.6mm, and 2mm according to the results of parametric optimization. The fixed constraints are applied to the fixed holes.

Under the assumption of small linear deformation, static structural simulation is adopted to obtain the guiding mechanism's stiffness in each direction. The force load is applied at the interface between the guiding mechanism and the PEA. The output displacement is simulated at the face where the guiding mechanism and the glass micropipette are connected. According to the computation of static structure analysis, the

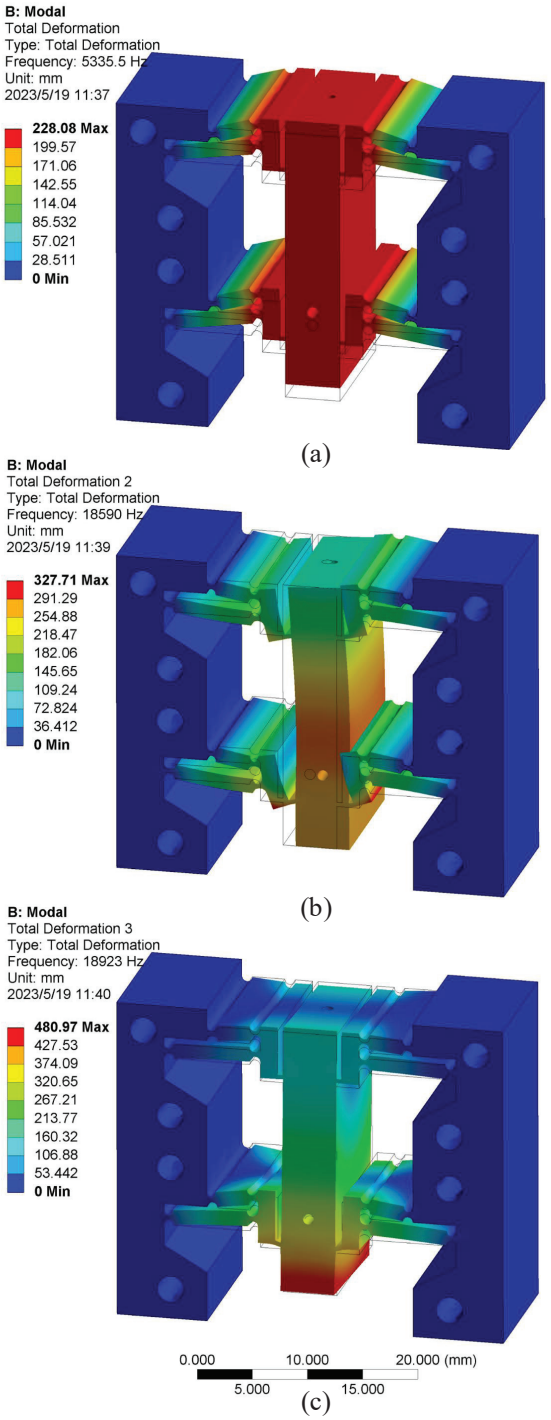

Fig. 6. The first-three modal shapes of the guiding mechanism in FEA. (a) the first-order modal shape, (b) the second-order modal shape, (c) the third-order modal shape.

stiffness in each direction is shown in Table II. The adopted coordinate system is shown in Fig. 1 where Y denotes the axial direction, X denotes the in-plane orthogonal direction and Z denotes the out-of-plane orthogonal direction. Off-axis stiffness ratio ($k_x/k_y, k_z/k_y$) is an effective criterion for evaluating the compliant mechanism's guiding performance. Non-functional stiffness should be as large as possible due to

TABLE III
SIMULATION RESULTS OF THE NATURAL FREQUENCIES OF THE GUIDING MECHANISM

Mode	1	2	3	4	5	6
Frequency (Hz)	5335.5	18590	18923	19931	26729	32924

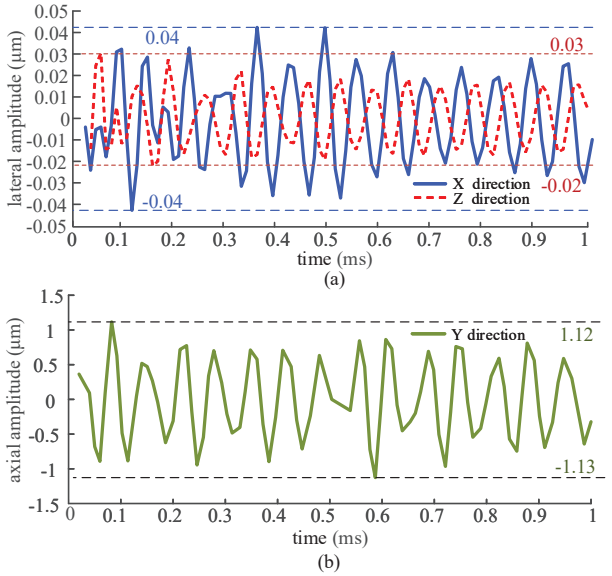

Fig. 7. Vibration of the guiding mechanism's output end in transient structural simulation at 15 kHz (a) in lateral direction, (b) in axial direction.

the need for high accuracy and small lateral vibration amplitude. The FEA static study demonstrates that the optimized guiding mechanism possesses a high off-axis stiffness ratio where $k_x/k_y = 11.36$ and $k_z/k_y = 14.79$.

Modal analysis is performed to obtain the natural frequencies of the guiding mechanism. Table III displays the first-six natural frequencies and Fig. 6 shows the first-three modal shapes.

B. Transient Structural Simulation

For the intent of evaluating the guiding mechanism's performance in decreasing the amplitude of lateral vibration, the transient response of the guiding mechanism is studied. In the simulation, a continuous sinusoidal displacement load was applied with a frequency of 15kHz. The input vibration amplitude in the x, y, and z directions are 0.1 μm, 0.5 μm, and 0.1 μm respectively. The vibration amplitude in each direction of the output end is shown in Fig. 7. The results show that the designed guiding mechanism can cut down the lateral vibration amplitude to less than 40% in the x direction and 25% in the z direction, which adequately meets the need of suppressing the lateral vibration in robotic vibration microinjection.

V. CONCLUSIONS

This paper proposes a novel lumped complaint guiding mechanism with double-notch right-circular flexure hinges for piezo-driven vibration cell microinjection which can

transmit the axial vibration and suppress the lateral vibration. The analytical kinematic modeling of the straight-line module is undertaken to certify the efficacy to conduct a straight-line motion of the designed compliant guiding mechanism, from which the movement trajectory and its numerical curvature are derived. The response surface optimization is adopted with the aim of improving the dynamic performance of the guiding mechanism. Finite element analysis based on ANSYS Workbench software set out to obtain the static and modal characteristics and to assess the effect on lateral vibration of the guiding mechanism. The guiding mechanism's off-axis stiffness ratio in the x direction and z direction are proved to be 11.36 and 14.79 respectively. The first-six-order natural frequencies are calculated and the first-three-order modal shapes are presented. With the actuation frequency of 15 kHz, the lateral vibration amplitudes in the x and z directions decreased to 40% and 25% respectively according to the transient structural simulation.

This paper demonstrates a new structure design for the manipulators of robotic piezo-driven vibration microinjection. Moreover, by replacing the glass micropipette with a cutting needle, the proposed guiding mechanism can be used for biological tissue cutting with similar requirements of small damage rupture tasks. But the adjustment range of the actuation frequency is limited. The performance and applicability of the proposed mechanism are desired to be further improved. In the future, the prototype will be fabricated to set up an experimental platform. Ideal control strategies will be investigated to evaluate the practical performance of the guiding mechanism further.

REFERENCES

[1] Z. Chi, Q. Xu, and L. Zhu, "A review of recent advances in robotic cell microinjection," *IEEE Access*, vol. 8, pp. 8520–8532, 2020.

[2] Y. Wei and Q. Xu, "A survey of force-assisted robotic cell microinjection technologies," *IEEE Transactions on Automation Science and Engineering*, vol. 16, no. 2, pp. 931–945, 2018.

[3] M. R. Capecchi, "High efficiency transformation by direct microinjection of dna into cultured mammalian cells," *Cell*, vol. 22, no. 2, pp. 479–488, 1980.

[4] A. Pillarisetti, M. Pekarev, A. D. Brooks, and J. P. Desai, "Evaluating the effect of force feedback in cell injection," *IEEE Transactions on Automation Science and Engineering*, vol. 4, no. 3, pp. 322–331, 2007.

[5] Z. Lu, X. Zhang, C. Leung, N. Esfandiari, R. F. Casper, and Y. Sun, "Robotic icsi (intracytoplasmic sperm injection)," *IEEE Transactions on Biomedical Engineering*, vol. 58, no. 7, pp. 2102–2108, 2011.

[6] W. Wang, X. Liu, D. Gelinas, B. Ciruna, and Y. Sun, "A fully automated robotic system for microinjection of zebrafish embryos," *PloS one*, vol. 2, no. 9, pp. 1–7, 2007.

[7] S. Zappe, M. Fish, M. P. Scott, and O. Solgaard, "Automated mems-based drosophila embryo injection system for high-throughput rnai screens," *Lab on a Chip*, vol. 6, no. 8, pp. 1012–1019, 2006.

[8] D. Abdelrahman, W. Hasan, and S. I. Da'As, "Microinjection quality control in zebrafish model for genetic manipulations," *MethodsX*, vol. 8, no. 7, p. 101418, 2021.

[9] P. Scherp and K. H. Hasenstein, "Microinjection–a tool to study gravitropism." *Advances in Space Research the Official Journal of the Committee on Space Research*, vol. 31, no. 10, pp. 2221–2227, 2003.

[10] H. Ladjal, J. L. Hanus, and A. Ferreira, "Micro-to-nano biomechanical modeling for assisted biological cell injection," *IEEE Transactions on Biomedical Engineering*, vol. 60, no. 9, pp. 2461–2471, 2013.

[11] K. Feng, Q. Xu, and L. M. Tam, "Design and development of a dexterous bilateral robotic microinjection system based on haptic feedback," *IEEE Transactions on Automation Science and Engineering*, vol. 20, no. 2, pp. 1452–1462, 2023.

[12] S. Permana, E. Grant, G. M. Walker, and J. A. Yoder, "A review of automated microinjection systems for single cells in the embryogenesis stage," *IEEE/ASME Transactions on Mechatronics*, vol. 21, no. 5, pp. 2391–2404, 2016.

[13] G. Fitzharris, J. Carroll, and K. Swann, "Electrical-assisted microinjection for analysis of fertilization and cell division in mammalian oocytes and early embryos - sciencedirect," *Methods in Cell Biology*, vol. 144, pp. 431–440, 2018.

[14] T. Fujishiro, T. Aoyama, K. Hano, M. Takasu, and Y. Hasegawa, "Microinjection system to enable real-time 3d image presentation through focal position adjustment," *IEEE Robotics and Automation Letters*, vol. 6, no. 2, pp. 4025–4031, 2021.

[15] G. Wang and Q. Xu, "Design and development of a piezo-driven microinjection system with force feedback," *Advanced Robotics*, vol. 31, no. 23-24, pp. 1349–1359, 2017.

[16] A. F. Ergenc, M. W. Li, M. Toner, J. D. Biggers, K. C. K. Lloyd, and N. Olgac, "Rotationally oscillating drill (ros-drill) for mouse icsi without using mercury," *Molecular Reproduction & Development*, vol. 75, no. 12, pp. 1744–1751, 2010.

[17] F. A. Khan, *Biotechnology fundamentals*. CRC Press, 2011.

[18] K. Ediz and N. Olgac, "Effect of mercury column on the micro-dynamics of the piezo-driven pipettes," *Journal of Biomechanical Engineering*, vol. 127, no. 3, pp. 531–535, 2005.

[19] H. Huang, J. K. Mills, C. Lu, and D. Sun, "A universal piezo-driven ultrasonic cell microinjection system," *Biomedical microdevices*, vol. 13, no. 4, pp. 743–752, 2011.

[20] W. Johnson, C. Dai, J. Liu, X. Wang, D. K. Luu, Z. Zhang, C. Ru, C. Zhou, M. Tan, and H. a. Pu, "A flexure-guided piezo drill for penetrating the zona pellucida of mammalian oocytes," *IEEE Transactions on Biomedical Engineering*, vol. 65, no. 3, pp. 678–686, 2017.

[21] J. Ling, T. Ye, Z. Feng, Y. Zhu, Y. Li, and X. Xiao, "A survey on synthesis of compliant constant force/torque mechanisms," *Mechanism and Machine Theory*, vol. 176, p. 104970, 2022.

[22] T. Ye, J. Ling, X. Kang, Z. Feng, and X. Xiao, "A novel two-stage constant force compliant microgripper," *Journal of Mechanical Design*, vol. 143, no. 5, p. 053302, 2021.

[23] C. Dai, L. Xin, Z. Zhang, G. Shan, T. Wang, K. Zhang, X. Wang, L.-T. Chu, C. Ru, and Y. Sun, "Design and control of a piezo drill for robotic piezo-driven cell penetration," *IEEE Robotics and Automation Letters*, vol. 5, no. 2, pp. 339–345, 2019.

[24] L. L. Howell, *Handbook of compliant mechanisms*. Handbook of Compliant Mechanisms, 2013.